19th Brazilian Congress of Thermal Sciences and Engineering
November 6th–10th, 2022, Bento Gonçalves - RS - Brazil

ENCIT-2022-0300
STUDY OF THE DYNAMICS OF STRATIFIED LIQUID-LIQUID HORIZONTAL PIPE FLOW VIA PARTICLE IMAGE VELOCIMETRY

P. J. Miranda-Lugo
Jorge E. Arrollo-Caballero
University of São Paulo (USP), São Carlos School of Engineering (EESC), Mechanical Engineering Department, Industrial Multiphase Flow Laboratory (LEMI), Av. Trab. São Carlense, 400 - Parque Arnold Schimidt, São Carlos - SP, 13566-590, Brazil.
pjosemiranda@usp.br*, jorgearrollo@usp.br

Marlon M. Hernandez-Cely
Engineering Center, Federal University of Pelotas, Rua Benjamin Constant, n° 989, Porto, Pelotas 96010-020, RS, Brazil.
marlonhc@usp.br

O. M. H. Rodriguez
University of São Paulo (USP), São Carlos School of Engineering (EESC), Mechanical Engineering Department, Industrial Multiphase Flow Laboratory (LEMI), Av. Trab. São Carlense, 400 - Parque Arnold Schimidt, São Carlos - SP, 13566-590, Brazil.
oscarmhr@sc.usp.br

Abstract. *Stratified liquid-liquid flow is a flow pattern observed in many industrial applications. The complexity of two-phase flow often limits rigorous numerical modeling of liquid-liquid flow in actual practice. One of the challenges is the prediction of velocity profiles related to the average velocities of the phases, pressure drop, and heat transfer. Another issue is the values of the shape factors, which are related to flow pattern transition. Several experimental studies have focused on measuring hydrodynamic characteristics of stratified liquid-liquid flows in horizontal or slightly inclined pipes; most works have focused on transitional/turbulent flow regimes for the oil and water phases. We will study the dynamics of a horizontal stratified oil-water pipe flow via Particle Image Velocimetry (PIV), Planar Laser-Induced Fluorescence (PLIF), and high-speed video recording. The PIV technique will be used to obtain non-intrusive instantaneous local velocity measurements of the lateral flow field, from which the mean axial and radial velocity components, root mean squared velocity, and Reynolds stresses can be estimated. The PLIF technique will provide the liquid-liquid interface shape. The interface's height will be determined by image processing algorithms. In order to offer a preliminary discussion on the dynamics of a horizontal stratified liquid-liquid pipe flow, without our experimental results, experimental data reported in the literature were collected and analyzed. The oil and water phases' laminar/transitional and turbulent/turbulent flow regimes were considered. For our ongoing experiments, we expect the mean velocity profiles to show both laminar and turbulent flow characteristics and interesting interfacial interactions between the phases. Regions of high-intensity turbulence are expected near the pipe wall and liquid-liquid interface. Furthermore, one may expect the presence of secondary flow.*

Keywords: *Oil-water flow, PIV, PLIF, Stratified flow, Velocity profile.*

1. INTRODUCTION

The flow of non-miscible liquids is frequent in many industrial applications, for instance, chemical, pharmaceutical, oil, energy, refrigeration, and food applications. The liquid-liquid two-phase flow may take different spatial configurations or flow patterns. These depend on many parameters, such as phase flow rates, fluids' physical properties, pipeline geometry, liquids holdup, wettability, and roughness of the tube. (Trallero *et al.*, 1997; Angeli and Hewitt, 2000; Rodriguez and Bannwart, 2008; Ibarra *et al.*, 2015; Chinaud *et al.*, 2017; Ahmed and John, 2018).

The liquid-liquid flow patterns are classified into disperses flow, intermittent flow, and separated flow. The latter includes core-annular flow and stratified flow. Such flow patterns are commonly modeled as parallel two-phase flows (Ooms *et al.*, 1983; Oliemans and Ooms, 1986; Boomkamp and Miesen, 1996; Joseph *et al.*, 1997; Trallero *et al.*, 1997; Bannwart, 2001; Rodriguez and Bannwart, 2006; Rodriguez and Baldani, 2012; Kushnir *et al.*, 2017). The most straightforward

configuration is the smooth stratified flow, an spatial arrangement where the lightest phase continuously flows over the heaviest phase. However, even in the most simplified geometry, this flow is still an open issue because of the problematic interactions at the interface, where several fluid dynamics mechanisms are involved (Ahmed and John, 2018; Ibarra *et al.*, 2018, 2021).

Many experimental studies have focused on the measurement of hydrodynamic characteristics of stratified liquid-liquid flows in horizontal or slightly inclined pipes; the works of Trallero (1995), Angeli and Hewitt (2000), Elseth (2001), Rodriguez and Oliemans (2006), Conan *et al.* (2007), Kumara *et al.* (2010), Amundsen (2011), Barmak *et al.* (2016), Ibarra *et al.* (2018), and Ibarra *et al.* (2021) stand out. Elseth (2001) investigated an oil-water flow in a horizontal steel pipe. The velocity profiles and turbulence characteristics of stratified flows were studied along the diametrical vertical plane via Laser Doppler Anemometry (LDA). Furthermore, gamma-ray measurements identified the local phase fractions of the flow.

Amundsen (2011) studied an oil-water flow at several inclinations (0°, $\pm 1^\circ$, $\pm 5^\circ$, and $\pm 10^\circ$, from the horizontal). The phases distributions in the diametrical vertical plane were measured by a gamma densitometer, while the LDA technique allowed measuring the velocity and turbulence distributions. The results indicated that the velocity profiles rely on the input water cut and tube inclination. For some situations, those authors noticed that the oil phase moved faster, even being the most viscous phase. This was because the wall shear stress in the oil layer was weaker than that of the water. That outcome agrees with the observations of Elseth (2001). Furthermore, the higher the input water cut, the more significant the tube inclination influence on the velocity profile, especially at higher angles.

In another interesting effort, Ibarra *et al.* (2018) examined the dynamics of horizontal liquid-liquid pipe flow using a simultaneous technique integrating Planar Laser-Induced Fluorescence (PLIF) and Particle Image/Tracking Velocimetry (PIV/PTV). The authors developed an experimental setup incorporating two laser-camera systems to record oil-water flows in smooth and wavy stratified flow patterns, covering laminar/transitional flow regimes for the oil and transitional/turbulent for the water phase. That study is the first attempt to collect spatial and temporal resolved in-situ local velocity (and phase) details at the pipe's vertical-central plane, spanning both liquid phases. Mean axial velocity profiles with laminar, transitional, and turbulent characteristics were obtained. Furthermore, the results revealed that the vertical velocity component can change the axial velocity profiles. Ibarra and coworkers also highlighted the reverse flow observed in the oil layer's center region represented by the signal changing of the mean vertical velocity component, which indicates the flow direction (toward the interface or moving away from it). That result was not reported in the experimental works of Kumara *et al.* (2010), and Amundsen (2011).

Recently, Ibarra *et al.* (2021) analyzed the pipe inclination influence on the hydrodynamic of an upward-inclined stratified oil-water flow using the same techniques and similar experimental conditions reported in their previous work (Ibarra *et al.*, 2018). The instantaneous velocity fields revealed complex flow structures in both phases, which promoted the emergence of interfacial waves with less stability as the pipe inclination increased. The results suggested that the interface waviness may modify the vertical velocity component. Moreover, the pipeline inclination influences the mean velocity profile, velocity fluctuations, and Reynolds stresses.

We study the stratified oil-water horizontal pipe flow dynamic using the two-dimensional PIV, PLIF, and high-speed video recording. The former technique will be used to obtain instantaneous local velocity measurements of the lateral flow field, from which the mean axial and radial velocity components, root mean squared velocity, and Reynolds stresses can be estimated. The PLIF technique will provide the liquid-liquid interface shape. The interface's height will be determined by image processing algorithms. To offer a preliminary discussion on the dynamics of a horizontal stratified liquid-liquid pipe flow, even without our experimental results, the experimental data presented in Tab. 1 were analyzed. For our ongoing experiments, which will be presented in the final version of this manuscript, we expect the mean velocity profiles to show both laminar and turbulent flow characteristics and interesting interfacial interactions between the phases. Regions of high-intensity turbulence are expected near the pipe wall and liquid-liquid interface. Furthermore, one may expect the presence of secondary flow.

Table 1. Flow conditions, geometrical and physical properties of experimental studies on the dynamic of stratified liquid-liquid horizontal pipe flow using the PIV and LDA techniques.

Author	Pipe material	e [mm]	θ [°]	D [mm]	μ_w [mPa·s]	μ_o [mPa·s]	σ [N/m]	ρ_w [kg/m^3]	ρ_o [kg/m^3]	C_w [–]	J_w [m/s]	J_o [m/s]	J_m [m/s]	$\frac{h_w}{D}$ [–]	Eo [–]	Re$_w$ [–]	Re$_o$ [–]
Elseth (2001)	Steel	0.045	60	56.3	1.00	1.64	0.043	997	785	0.75	0.74	0.26	1.02	0.644	38	50 722	18 155
Kumara *et al.* (2010)	Steel	0.045	60	56.0	1.00	1.64	0.043	996	790	0.50	0.25	0.25	0.5	0.490	37	22 588	10 692
Amundsen (2011)	Steel	0.045	60	56.3	1.02	1.64	0.043	1000	790	0.25	0.25	0.75	1.0	0.322	38	32 881	23 696
Ibarra *et al.* (2018)	Quartz	0.001	30	32.0	0.90	5.40	0.035	998	824	0.20	0.08	0.32	0.4	0.290	12	6895	1745
Present work	Glass	0.001	30	20.5	1.00	1.56	0.043	995	820	–	–	–	–		4	–	–

2. EXPERIMENTAL WORK

2.1 Experimental setup

One can see in Fig. 1 a schematic view of the new test facility designed and built up to study the dynamics of stratified liquid-liquid flow. Water (ρ_w = 995 kg/m^3, μ_w = 1.0 mPa·s) and oil (ρ_o = 820 kg/m^3, μ_o = 1.64 mPa·s) were adopted as working fluids. There are two independent supply lines, one for water and another for oil, and two test sections (F and K), made of borosilicate-glass pipes with lengths (L_p) of 4.5 and 7.5 m and internal diameters (D) of 9.7 and 20.5 mm, respectively. Each test section has a rectangular transparent acrylic viewing section (G and L), where the PIV system and a high-speed video camera will be installed. The fluid distribution system is driven by gravity from two reservoirs (A and B). The liquids are injected into the test section through a set of flow straighteners (C, D, H, and I) and a specially designed inlet section (E and J). The former aims to reduce large-scale flow structures at the test section inlet, while the latter prevents the fluids from mixing inside it and promotes stratified flow once the liquids get together in the test section. Details of the flow straighteners and the inlet section are presented in Fig. 2. Both flow lines have an array of liquid flowmeters (1, 2, 4, 5), thermocouples type K (3, 6, 7, 8), and differential pressure transducers (9, 10). The two-phase mixture that comes from the test section is transferred to an oil-water separator (M). From this separator, each fluid is driven to tanks (N and Q) and then pumped by positive displacement pumps (P and S), controlled by variable-frequency drivers (O and R), to their respective reservoirs (A and B), completing the test loop. The liquids' columns in reservoirs A and B are controlled through gauge pressure sensors installed in each tank. A control system based on LabVIEW® will allow setting the water and oil flow rates, selecting the appropriate pumps and flowmeters, and checking in real-time the experimental conditions. Images of the oil-water stratified flow in the lateral and cross-section views will be taken separately using a high-speed video camera. Image processing algorithms will be applied to the collected images to obtain two-phase velocity profiles, turbulence statistics, and the interface's longitudinal (R_1) and cross-section (R_2) curvature.

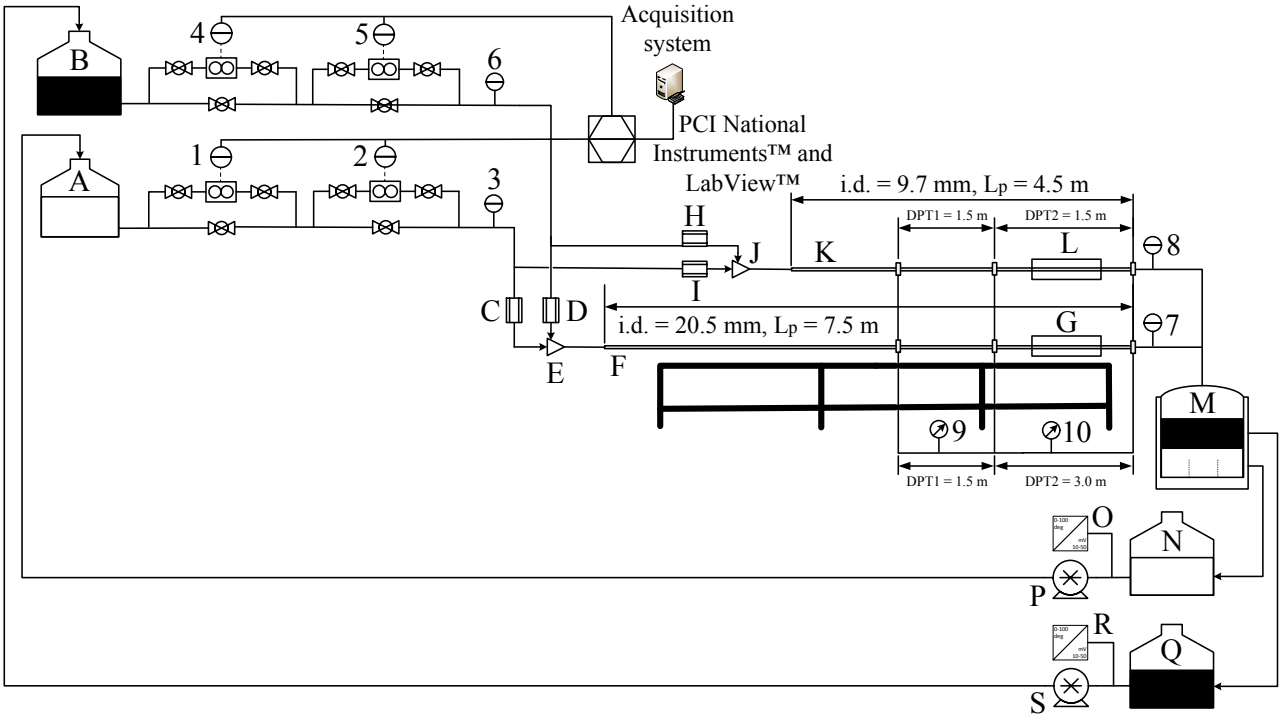

Figure 1. Schematic representation of the liquid-liquid test facility installed at the Industrial Multiphase Flow Laboratory (LEMI) of the University of São Paulo (USP) at the São Carlos campus.

2.2 Experimental procedure

The experimental campaign will focus on the study of the dynamics of stratified laminar-laminar and turbulent-turbulent horizontal pipe flow in a broad range of Reynolds numbers via PIV and the identification of the liquid-liquid interface's shape by PLIF technique. Once the liquid distribution is driven by gravity and consider that the stratified flow is only observed in condition where it is stable, appropriate oil and water's superficial velocities (J_o and J_w) should be set into the stratified region of the flow pattern map corresponding to our experimental conditions. The flow pattern map for liquid-liquid horizontal pipe flow for two i.d. pipes of 20.5 and 9.7 mm was drawn using the one-dimensional liquid-liquid flow model model proposed by Rodriguez and Castro (2014) and can be seen in Fig. 3. That model takes into account

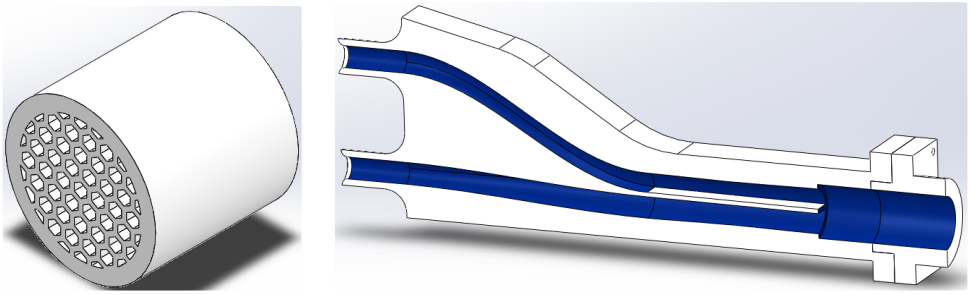

(a) (b)

Figure 2. (a) Flow straightener to reduce large-scale flow structures upstream of the the test section inlet, (b) Inlet section to prevent the fluids mixing and to promote stratified flow at the test section.

a wavy, concave, or convex interface as a function of the Eötvös number, interface height, and contact angle is used to calculate the in-situ average quantities of the flow, such as the phases' Reynolds numbers and liquid holdups.

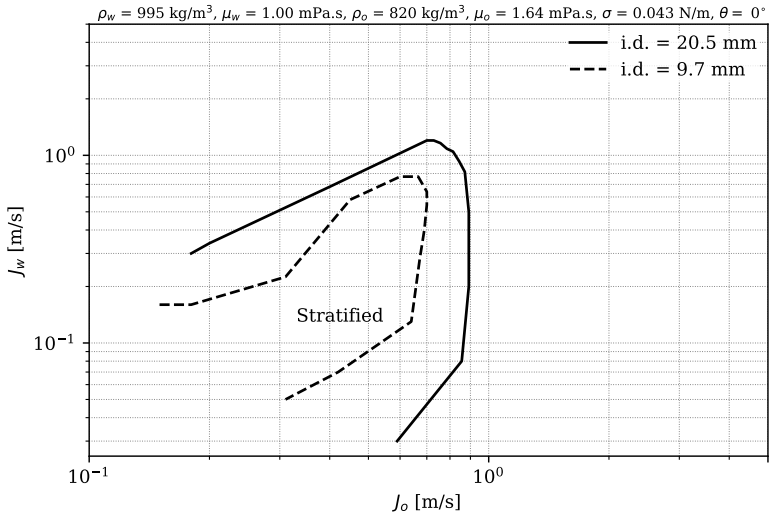

Figure 3. Flow pattern map for liquid-liquid horizontal pipe flow. The solid lines represents the boundary between the stratified and churning flows for the pipe of internal diameter (i.d.) equal to 20.5 mm, while the dashed line indicates the same boundary but for the i.d. = 9.7 mm. J_o and J_w refer to the oil and water's superficial velocities, respectively. The parameter ρ, μ and σ represent density, dynamic viscosity and oil-water surface tension, respectively. The subscripts w and o refer to the water and oil phases. The test section inclination θ is measured from the horizontal.

Since the liquid-liquid interface scatters the laser sheet (Nd:YAG laser with wavelength of 532 nm) of the PIV system and the laser's direction change due to the mismatch of the fluids' refractive index (Snell's law), the assessment of the dynamic of the stratified flow via PIV technique will be carried out separately for each fluid, i.e., the oil and water phases will be studied non-simultaneously. The PLIF technique will be used to identify the liquid-liquid interface's shape and its longitudinal curvature radius. To combine the two techniques, hollow glass–spheres with a mean diameter of 10 μm and a density of 1,100 kg/m^3, and silver coated glass spheres with a mean diameter of 50 μm and a density of 800 kg/m^3, will be seeded into the water and oil phases, respectively. In addition, rhodamine 6G will be added to the water phase to obtain a clear distinction between the phases and, therefore, to identify clearly the liquid–liquid interface. The choice of the fluorescent dye for the PLIF technique was based on the excitation and emission spectra. We found that rhodamine 6G has an excitation peak in a wavelength of 530 nm (green light) and an emission peak at 552 nm (yellow light). Figure 4 described the setup for data collection procedure. To study the water phase's dynamic, the laser sheet will be located under the viewing section towards the bottom up, while for the oil phase the laser will be installed above the viewing section towards top to bottom. An array of high-speed video camera Olympus i-Speed3, suitable lens, and a high-pass filter with cut frequency of 550 nm will be used to block the scattered light from the liquid-liquid interface and the hollow glass–spheres at 532 nm (green light). In addition, pressure drop data for single-phase and two-phase flows will be also collected during the experiments.

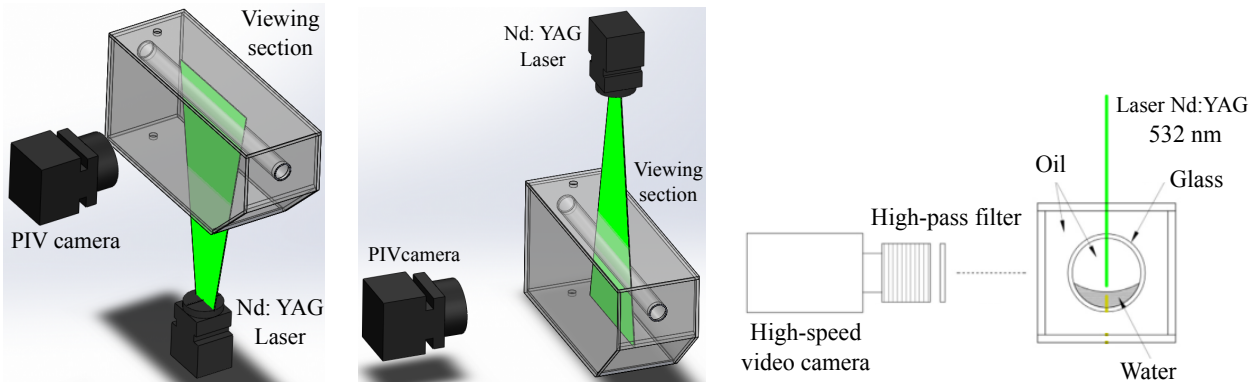

(a) (b) (c)

Figure 4. Data collection methodology. (a) Assesment of the water phase's dynamic, (b) Assesment of the oil phase's dynamic, (c) Configuration of high-speed video camera, high-pass filter, and viewing section for execution of PIV and PLIF techniques.

2.3 Processing and data analysis

The instantaneous velocity data obtained by the PIV technique will be analyzed in order to assess the hydrodynamic of the stratified flow. Since the oil and water phases will be studied separately, the experimental data processing will be also evaluate independently for each phase. The time-mean local axial $\langle u \rangle$ and radial $\langle v \rangle$ velocity components are calculated by Eq. 1.

$$\langle u \rangle = \frac{1}{n}\sum_{i=1}^{n} u_i \qquad \text{and} \qquad \langle v \rangle = \frac{1}{n}\sum_{i=1}^{n} v_i \tag{1}$$

where n represents the number of instantaneous velocity data (number of images), u_i and v_i are the instantaneous and local axial and radial velocity components, respectively. On the other hand, the standard deviation of the local velocity components, or velocity fluctuation rms (root mean squared) are estimated by Eq. 2.

$$u_{rms} = \sqrt{\frac{1}{n}\sum_{i=1}^{n} \left(u_i - \langle u \rangle\right)^2} \qquad \text{and} \qquad v_{rms} = \sqrt{\frac{1}{n}\sum_{i=1}^{n} \left(v_i - \langle v \rangle\right)^2} \tag{2}$$

The cross-moments are defined by Eq. 3. Here, $u\prime$ and $v\prime$ represent the velocity fluctuation components in streamwise and wall normal directions. The Reynolds shear stress is obtained by multiplying the cross-moments and the liquid density ($\rho \langle u\prime v\prime \rangle$).

$$\langle u\prime v\prime \rangle = \langle uv \rangle - \langle u \rangle \langle v \rangle = \frac{1}{n}\sum_{i=1}^{n} \left(u_i - \langle u \rangle\right)\left(v_i - \langle v \rangle\right) \tag{3}$$

2.4 Validation of experimental result

The experiments will be validated consider single-phase laminar flow. The time-mean local axial velocity profile obtained from the PIV technique will be compared with the Hagen-Poiseuille's analytical solution given by Eq. 4.

$$u(r) = \frac{R^2}{4\mu}\frac{\Delta P}{\Delta L}\left(1 - \frac{r^2}{R^2}\right) \tag{4}$$

where μ represents the liquid dynamic viscosity, ΔP is the pressure drop measured experimentally, ΔL is the distance between the pressure taps, R is the pipe radius, and r represents the radial coordinate.

The shear stress distribution will be calculated from derivation the Eq. 4 with respect to the radial coordinate r and multiplying by the dynamic viscosity μ, resulting in Eq. 5.

$$\tau = -\frac{r}{2}\frac{\Delta P}{\Delta L} \tag{5}$$

For single-phase turbulent flow, the experimental velocity profile will be compared with the power-law velocity profile defined by Eq. 6. Here, $u(r)$ is the velocity profile and u_{max} states the maximum experimental velocity. The factor N is a function of the Reynolds number.

$$\frac{u(r)}{u_{max}} = \left(1 - \frac{r}{R}\right)^{1/N} \tag{6}$$

In this case, the flow shear stress will be determined by adding the laminar shear stress (τ_{lam}) and turbulent shear stress (τ_{turb}), as defined in Eq. 7.

$$\tau = \tau_{lam} + \tau_{turb} = \mu \frac{d\bar{u}}{dy} - \rho \overline{u'v'} \tag{7}$$

The experimental two-phase flow results of the present work will be compared compared with those reported by Elseth (2001), Kumara *et al.* (2010), Amundsen (2011) and Ibarra *et al.* (2018) using the PIV/PTV, PLIF, LDA, and gamma densitometry techniques with the flow conditions, geometrical and physical properties described in Tab. 1.

3. EXPECTED RESULTS

This section presents the identification of the interface's height and longitudinal curvature, as well as measurements of mean axial and radial velocities, streamwise and normal velocity fluctuations, cross-moments and Reynolds stresses of similar experimental studies reported in the literature. A set of three mixture velocities and four water cuts are analyzed in order to explore the dynamic of the stratified liquid-liquid flow under different flow conditions.

3.1 Determination of the interface's height and longitudinal curvature via PLIF

An image of the longitudinal view of the interface is presented in Fig. 5. A median filter and thresholding are applied to the original images. The first white pixel found from a bottom-up scanning process of each binary image column defines the liquid-liquid interface. Once the latter is known, one can identify the interface's maximum and minimal local points, see Fig. 5(b). The curvatures that contain the minimal local points are used to fit circles through the least-squares method. The interface's longitudinal curvature radius (R_1) is determined by a probability density function (PDF) of the circles' size.

(a) (b)

Figure 5. Image processing to determine the curvature of the interface in the flow direction (R_1). (a) Original image extracted from de Castro and Rodriguez (2015). (b) Identification of the liquid-liquid interface and maximum and minimal local points (blue asterisks). The black color in (b) represents water, and the white color refers to oil.

3.2 Dynamics of stratified liquid-liquid horizontal pipe flow via PIV

One can see in Fig. 6 the measurements of mean axial and radial velocities, streamwise and normal velocity fluctuations, cross-moments and Reynolds stresses for the stratified oil-water horizontal flow studied by Kumara *et al.* (2010) and Ibarra *et al.* (2018). The two-phase axial velocity profile showed in Fig. 6(a) is fairly flat since both phases are fully turbulent. Therefore, the shear rates near the liquid-liquid interface are small. The maximum mean axial velocity is observed in the oil phase, which is explained once in turbulent flows as this case, the density ratio counteracts the viscosity effect. The maximum mean axial velocity of the stratified flow was around 0.63 m/s and it is located at the normalized radial position 0.42. On the other hand, the root mean-squared velocity fluctuations of the axial (u_{rms}) and vertical (v_{rms}) direction and the Reynolds stress ($\rho \langle u'v' \rangle$) have higher values in regions with larger axial velocity gradient. Considering the u_{rms}, two peaks with values of 0.10 and 0.59 m/s are observed close to the wall, which corresponds to 20% of the mixture velocity (J_m = 0.5 m/s) and indicates that the axial velocity fluctuation is intimate related to the mean shear. The vertical velocity fluctuation v_{rms} is less than the axial fluctuation over the entire normalized radial positions. The delay between the axial and normal velocity fluctuations suggests that large fluctuations in the streamwise direction play an important role in the turbulence production. The v_{rms} values are suppressed due to the impenetrability of the pipe. Therefore, the maximum mean vertical fluctuation is observed farther from the pipe wall compared to the axial fluctuation. One can see that the fluctuation's magnitude decreases from their maximum values in direction to the bulk of each phase due to processes of

diffusion and turbulence transport. The oil-water interface represents a moving wall and the stable density stratification suppresses turbulent fluctuations normal to the interface. However, the results indicated that near the interface, both axial and normal velocity fluctuations increase because of the interfacial shear stress and the presence of small interfacial waves, respectively. The Reynolds stress is proportional to the mean shear rate and presents two peaks located almost at the same radial position of the vertical fluctuations' peaks. This is explained by the reduction of v_{rms} near the pipe wall. Since the two-phase axial velocity profile is fairly flat between the normalized radial position -0.20 and 0.52, the mean shear rate is quite small, furthermore, the density stratification near the interface suppresses the normal velocity fluctuations. Therefore, the Reynolds stress calculated from PIV measurements decreases towards zero close to the liquid-liquid interface, which agrees with the Boussinesq eddy viscosity hypothesis.

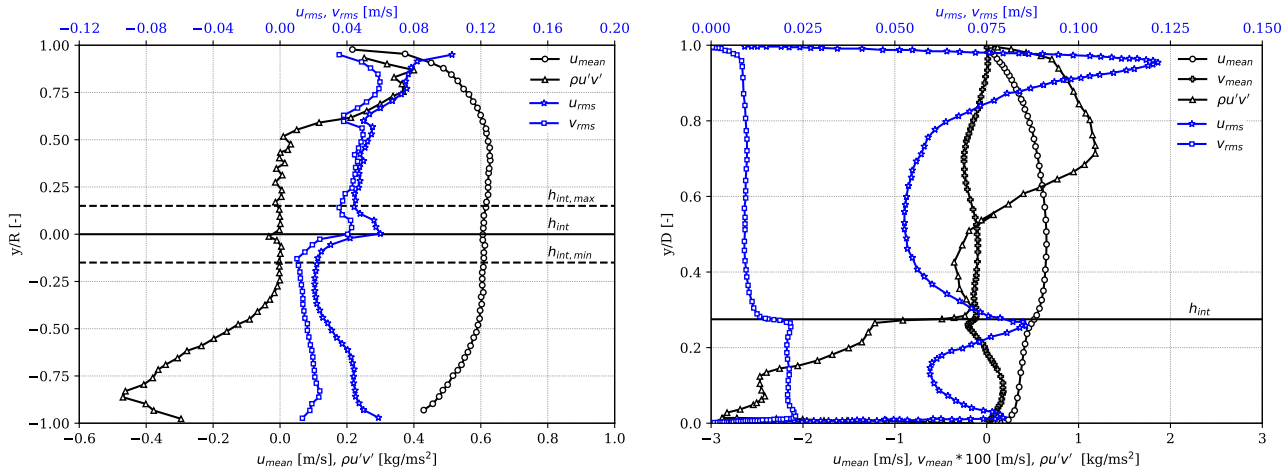

(a) (b)

Figure 6. Mean axial and vertical velocity profiles, and turbulence statistics for stratified oil-water horizontal flow at (a) J_m = 0.5 m/s and C_w = 0.5, $\mathrm{Re_w}$ = 22,588 and $\mathrm{Re_o}$ = 10,692 and (b) J_m = 0.4 m/s and C_w = 0.2, $\mathrm{Re_w}$ = 6,895 and $\mathrm{Re_o}$ = 1,745. Experimental data extracted from (a) Kumara *et al.* (2010) and (b) Ibarra *et al.* (2018).

One can observed in Fig. 6(b) the two-phase axial and radial velocity profiles and the turbulence statistics of the flow conditions studied by Ibarra *et al.* (2018). In this case, the water phase flows in the turbulent regime whereas the oil phase flows in the laminar/transitional regime, with similar mixture velocity but a lower water cut than that adopted by Kumara *et al.* (2010). The shape of the two-phase mean axial velocity profile (u_{mean}) is still relatively flat and also with a maximum velocity around 0.65 m/s in the oil phase, near the center of the pipe. The corresponding mean vertical velocity profile (v_{mean}) indicates oil and water flows downward and upward towards the liquid-liquid interface region, respectively. Even though, the mean vertical velocity profile is not strong enough to modify the shape of the mean axial velocity. The oil-water interface is located at normalized radial position of 0.26 as indicated by the horizontal solid lines called h_{int}. Differently from Fig. 6(a), the interface height was almost constant over the entire sampling time, which results in an average absolute deviation of 1.2% for the mean interface height. Therefore, the dashed lines showed in the earlier case are not presented for the Ibarra's data.

The velocity fluctuation or standard deviation in the axial direction (u_{rms}) can be seen in Fig. 6(b). Similar to Fig. 6(a), peaks are clearly observed in regions close to the pipe wall and the liquid-liquid interface, and minimum values in the bulk of each phase. One can notice that the water phase has greater vertical velocity fluctuation than the oil phase as result of the turbulence in the water's bulk. This is at odds with axial velocity fluctuations described by Kumara *et al.* (2010) and might be related to the water cut difference, in other words, it might be associated to the restricted water layer cross-section flow area. Furthermore, the difference between the axial an vertical velocity fluctuations (u_{rms}) is greater for the flow conditions tested by Ibarra *et al.* (2018). The vertical fluctuation for the laminar/transitional oil flow are quite reduced toward zero, while the turbulent water flow also presents a reduction of the vertical velocity fluctuation values but they keep still larger than the oil phase. One can notice that the profiles of (u_{rms}) are similar to the axial velocity fluctuation, with pea close the pipe wall and the liquid-liquid interface. Nevertheless, another region of high turbulence can be seen in the water's bulk. This may be explained due to the presence of secondary flow structures as suggested by changes in the water radial component velocity. The Reynolds stress $(\rho \langle u\prime v\prime \rangle)$ is also shown in Fig. 6(b). The maximum magnitude of the Reynolds stress is observed in the water phase, which flows in turbulent regime. This agrees with the results of Fig. 6(a). However, in the present case, Reynolds stress maximum in the water phase is found near the pipe wall, unlike the oil phase, where it is located in a normalized radial position farther from the pipe wall.

Figure 7 depicts experimental results extracted from Elseth (2001), obtained via LDA and gamma densitometry techniques. The vertical mean velocity profile is not presented since those authors did not measure the radial velocity

component. The flow conditions considered turbulent/turbulent oil-water phases with equal mixture velocity but different water cut. Once both phases flow in turbulent regime, the two-phase axial velocity profile is flat with a maximum velocity around 1.30 m/s in the water phase. The velocity fluctuation in the straemwise direction (u_{mean}) are also presented. As also observed in Fig. 6(b), three peaks of the axial velocity fluctuation with values of 0.06, 0.18, and 0.22 m/s at radial positions near to the pipe wall and the oil-water interface. In this case, the interface mean height was located at a normalized position around 0.4 and were observed disturbances caused by the presence of interfacial waves and droplets, which results in a broad interface with normalized radial positions varying between 0.2 to 0.6 as indicated by the dashed lines $h_{int,max}$ and $h_{int,min}$. One can notice that the u_{rms} values are not lowest in the pipe center as in single-phase flow, an explanation is the lowest mean velocity gradients for two-phase flow to be located in radial positions far away from the center pipe, since it depends on the water cut. On the other hand, the vertical velocity fluctuations (v_{rms}) also revealed three peaks, whose normalized radial positions agree with those of the axial velocity fluctuations, however the values obtained for the vertical fluctuations are lower than the those of the streamwise direction.

The cross-moments $(\langle u\prime v\prime \rangle)$ and the Reynolds stress $(\rho \langle u\prime v\prime \rangle)$ are also described in Fig. 7. It is possible to observe two peaks near the pipe wall almost at the same normalized radial position of the vertical fluctuations' peaks. However, differently from the previous cases, the magnitude of the maximum Reynolds stress is found in the oil phase, which has a reduced cross-sectional area. The interface region reveals a higher turbulence intensity in the water phase than in the oil phase. A comparison between the cross-moment and Reynolds shear distributions reveals the role of the liquid density on the turbulence intensity in the interface region.

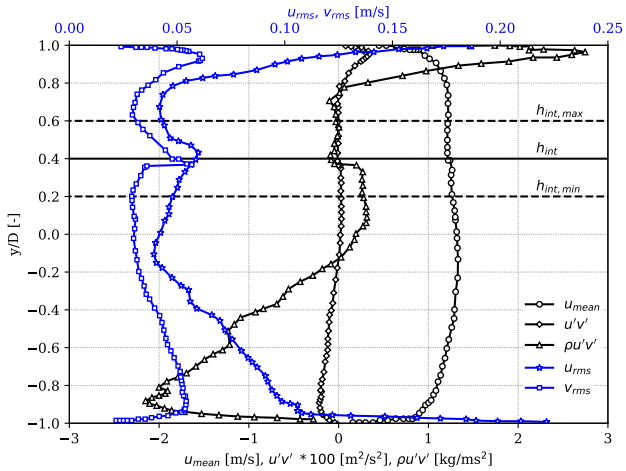

Figure 7. Mean axial and vertical velocity profiles, and turbulence statistics for stratified oil-water horizontal flow at (a) J_m = 1.02 m/s and C_w = 0.75, $\mathrm{Re_w}$ = 50,722 and $\mathrm{Re_o}$ = 18,155. Experimental data extracted from Elseth (2001).

4. CONCLUSIONS

The understanding of the dynamics of a horizontal stratified oil-water pipe flow is fundamental step to shed light on stability analysis of liquid-liquid separated flows that allows the modeling of flow-pattern transition. In this work, the dynamics of a horizontal stratified oil-water pipe flow via PIV, PLIF, and high-speed video recording is studied. Experimental data reported in the literature with laminar/transitional and turbulent/turbulent flow regimes for the oil and water phases were collected and analyzed. The results considered the mean axial and radial velocity components, root mean squared velocity or velocity fluctuations, cross-moments, and Reynolds stress. Similarities with the dynamics of single-phase flow were stood out. The results suggested that strong vertical velocity components may modify the shape of the axial velocity profiles. For our ongoing experiments, image processing algorithms will be used to provide statistical information on the shape of the liquid-liquid interface. Furthermore, it is expected the mean velocity profiles to show both laminar and turbulent flow characteristics and interesting interfacial interactions between the phases. Regions of shear with high-intensity turbulence are expected close to the pipe wall and at the liquid-liquid interface. The larger the cross-section curvature of the interface, the stronger the influence of secondary flow on the stratified flow pattern transition.

5. ACKNOWLEDGEMENTS

The authors gratefully acknowledge CAPES (Coordination of the Improvement in Higher Level Personnel of Brazil) for the grants of Pedro J. Miranda-Lugo (proc. 88882.379164/2019-01), and National Council for Scientific and Technological (CNPq) for Jorge E. Arrollo-Caballero and Oscar M. H. Rodriguez's grants (proc. 131659/2021-9 and proc. 311057/2020-9, respectively). Sincere thanks are extended to Mr. Pedro Donizete, Mr. Lázaro D. Bernardo, and Mr. Jorge N. dos Santos

for their technical support during the built up of the experimental rig.

6. REFERENCES

Ahmed, S.A. and John, B., 2018. "Liquid–liquid horizontal pipe flow–a review". *Journal of Petroleum Science and Engineering*, Vol. 168, pp. 426–447.

Amundsen, L., 2011. *An experimental study of oil-water flow in horizontal and inclined pipes*. Ph.D. thesis, The Norwegian University of Science and Technology (NTNU), Trondheim.

Angeli, P. and Hewitt, G., 2000. "Flow structure in horizontal oil–water flow". *International Journal of Multiphase Flow*, Vol. 26, No. 7, pp. 1117–1140.

Bannwart, A.C., 2001. "Modeling aspects of oil–water core–annular flows". *Journal of Petroleum Science and Engineering*, Vol. 32, No. 2, pp. 127–143.

Barmak, I., Gelfgat, A., Vitoshkin, H., Ullmann, A. and Brauner, N., 2016. "Stability of stratified two-phase flows in horizontal channels". *Physics of Fluids*, Vol. 28, No. 4, p. 044101.

Boomkamp, P. and Miesen, R., 1996. "Classification of instabilities in parallel two-phase flow". *International Journal of Multiphase Flow*, Vol. 22, pp. 67–88.

Chinaud, M., Park, K.H. and Angeli, P., 2017. "Flow pattern transition in liquid-liquid flows with a transverse cylinder". *International Journal of Multiphase Flow*, Vol. 90, pp. 1 – 12. ISSN 0301-9322.

Conan, C., Masbernat, O., Décarre, S. and Liné, A., 2007. "Local hydrodynamics in a dispersed-stratified liquid–liquid pipe flow". *AIChE Journal*, Vol. 53, No. 11, pp. 2754–2768.

de Castro, M.S. and Rodriguez, O.M., 2015. "Interfacial waves in stratified viscous oil–water flow". *Experimental Thermal and Fluid Science*, Vol. 62, pp. 85–98.

Elseth, G., 2001. *An experimental study of Oil/water flow in horizontal pipes*. Ph.D. thesis, The Norwegian University of Science and Technology (NTNU), Porsgrunn.

Ibarra, R., Matar, O., Markides, C., Zadrazil, I. *et al.*, 2015. "An experimental study of oil-water flows in horizontal pipes". In *Proceedings...* BHR Group, 17th International Conference on Multiphase Production Technology, Cannes, France, pp. 169–183.

Ibarra, R., Matar, O.K. and Markides, C.N., 2021. "Experimental investigations of upward-inclined stratified oil-water flows using simultaneous two-line planar laser-induced fluorescence and particle velocimetry". *International Journal of Multiphase Flow*, p. 103502.

Ibarra, R., Zadrazil, I., Matar, O.K. and Markides, C.N., 2018. "Dynamics of liquid–liquid flows in horizontal pipes using simultaneous two–line planar laser–induced fluorescence and particle velocimetry". *International Journal of Multiphase Flow*, Vol. 101, pp. 47 – 63. ISSN 0301-9322.

Joseph, D.D., Bai, R., Chen, K.P. and Renardy, Y.Y., 1997. "Core-annular flows". *Annual Review of Fluid Mechanics*, Vol. 29, No. 1, pp. 65–90.

Kumara, W., Halvorsen, B. and Melaaen, M., 2010. "Particle image velocimetry for characterizing the flow structure of oil–water flow in horizontal and slightly inclined pipes". *Chemical engineering science*, Vol. 65, No. 15, pp. 4332–4349.

Kushnir, R., Segal, V., Ullmann, A. and Brauner, N., 2017. "Closure relations effects on the prediction of the stratified two-phase flow stability via the two-fluid model". *International Journal of Multiphase Flow*, Vol. 97, pp. 78–93.

Oliemans, R.V.A. and Ooms, G., 1986. "Core-annular flow of oil and water". *Multiphase Science and Technology*, Vol. 2, No. 1-4, pp. 427–476. ISSN 0276-1459.

Ooms, G., Segal, A., van der Wees, A., Meerhoff, R. and Oliemans, R., 1983. "A theoretical model for core-annular flow of a very viscous oil core and a water annulus through a horizontal pipe". *International Journal of Multiphase Flow*, Vol. 10, No. 1, pp. 41–60.

Rodriguez, O. and Baldani, L., 2012. "Prediction of pressure gradient and holdup in wavy stratified liquid–liquid inclined pipe flow". *Journal of Petroleum Science and Engineering*, Vol. 96, pp. 140–151.

Rodriguez, O. and Bannwart, A., 2006. "Experimental study on interfacial waves in vertical core flow". *Journal of Petroleum Science and Engineering*, Vol. 54, No. 3-4, pp. 140–148.

Rodriguez, O. and Oliemans, R., 2006. "Experimental study on oil–water flow in horizontal and slightly inclined pipes". *International Journal of Multiphase Flow*, Vol. 32, No. 3, pp. 323–343.

Rodriguez, O.M. and Bannwart, A.C., 2008. "Stability analysis of core-annular flow and neutral stability wave number". *AIChE Journal*, Vol. 54, No. 1, pp. 20–31.

Rodriguez, O.M. and Castro, M.S., 2014. "Interfacial-tension-force model for the wavy-stratified liquid–liquid flow pattern transition". *International Journal of Multiphase Flow*, Vol. 58, pp. 114–126.

Trallero, J.L., Sarica, C. and Brill, J.P., 1997. "A Study of Oil-Water Flow Patterns in Horizontal Pipes". *SPE Production & Facilities*, Vol. 12, No. 03, pp. 165–172.

Trallero, J.L., 1995. *Oil-water flow patterns in horizontal pipes*. Doctor of philosophy in petroleum engineering, The University of Tulsa, Tulsa.

7. RESPONSIBILITY NOTICE

The authors are solely responsible for the printed material included in this paper.

NOMENCLATURE

Acronyms

LDA	Laser doppler anemometry
PIV	Particle image velocimetry
PLIF	Planar laser-induced fluorescence
PTV	Particle tracking velocimetry

Subscripts

int	Mean interface
int, max	Maximum interface
int, min	Minimum interface
lam	Laminar
m	Mixture
o	Oil phase
p	Pipe
$turb$	Turbulent
w	Water phase

Greek symbols

θ	Contact angle	[degrees]
μ	Dynamic viscosity	[mPa·s]
σ	Surface tension	[N/m]
ρ	Density	[kg/m^3]
τ	Shear stress	[Pa]

Latin symbols

C	Water cut	[–]
D	Internal diameter	[mm]
e	Roughness	[m]
Eo	Eotvos number	[–]
h	Interface's height	[m]
J	Superficial velocity	[m/s]
L	Lenght	[m]
ΔL	Distance between the pressure taps	[m]
n	Number of instantaneous velocities	[m/s]
N	Factor of the single-phase turbulent velocity profile	[–]
ΔP	Pressure drop measured experimentally	[Pa]
R	Pipe radius	[m]
Re	Reynolds number	[–]
$u(r)$	Axial velocity profile	[m/s]
u_{max}	Maximum axial velocity	[m/s]
$\langle u \rangle$	Time-mean local axial velocity component	[m/s]
u_i	Instantaneous local axial velocity component	[m/s]
$\langle v \rangle$	Time-mean local radial velocity component	[m/s]
v_i	Instantaneous local radial velocity component	[m/s]
u_{rms}	Axial velocity fluctuation	[m/s]
v_{rms}	Radial velocity fluctuation	[m/s]
$\langle u\prime v\prime \rangle$	Cross-moments	[m^2/s^2]
$\rho \langle u\prime v\prime \rangle$	Reynolds shear stress	[kg/m.s^2]